Effective Focal Area Dimension Optimization of Shear Horizontal Point-Focusing EMAT Using Orthogonal Test Method

Hongyu Sun, Lisha Peng, *Student Member, IEEE*, Shen Wang, Qing Wang, *Senior Member, IEEE*, Wei Zhao, and Songling Huang, *Senior Member, IEEE,*

Abstract—**To overcome the shortcomings of low energy conversion efficiency of electromagnetic acoustic transducers (EMATs), point-focusing shear horizontal (PFSH) wave EMAT is used to focus the wave energy into a specific area. Many factors will affect the capability of the focusing transducer, and in addition to considering the signal intensity, the detection accuracy is also required to be investigated. Specifically, to simplify the test process, we use the orthogonal test method to study the effect of different influence parameters on signal intensity and focal area dimensions. Seven factors are selected, and three results are determined in the test. Range analysis shows that for signal amplitude M, the top three impact factors are the coil width w, coil turns n, and focal length lF (equal to bandwidth factor α). Moreover, magnet number m and frequency f_c dominate the effective focal length l_{fd}, and aperture angle θ determines the effective focal width w_{fd}. To enable higher signal intensity and smaller focal area dimensions, it is necessary to consider various factors on the PFSH-EMAT focusing performance. The test's signal intensity with optimized parameters' combination at the focal point is nearly 144.42% higher than the average of all the tests, l_{fd} decreased by 37.84%, and w_{fd} decreased by 50.59%. The experiment also verified that focusing EMAT with optimized parameters has a better focusing performance.**

***Index Terms*—Focal area dimensions, orthogonal test, parameter optimization, point-focusing shear horizontal electromagnetic acoustic transducer (PFSH-EMAT).**

I. INTRODUCTION

ELECTROMAGNETIC acoustic transducers (EMATs) are currently used in nondestructive evaluation (NDE) of steel plates and pipes due to their noncontact, high speed, and application in high-temperature environment [1]-[5]. Compared with piezoelectric ultrasonic transducers, EMAT is more versatile and more accessible to be used in the field of NDE because it does not require a couplant [6]. [7]. Through different combinations of the coil and permanent magnets, EMAT could generate waves of different modes in the specimen: shear vertical (SV) body waves, shear horizontal (SH) guided waves, longitudinal waves, Rayleigh surface waves, and Lamb waves. Moreover, the structure of the EMAT is different for different ultrasonic generation mechanisms. Its excitation mechanism mainly includes Lorentz forces, magnetization forces, and magnetostriction effects, and the latter two only exist in ferromagnetic materials [8]–[11].

As one of the SH guided wave modes, the SH0 mode wave has many advantages: little attenuation of signal intensity when it encounters defects, no mode conversion occurs, and there is no dispersion phenomenon, which is beneficial to the extraction and analysis of the ultrasonic guided wave detection signal [12], [13]. Based on the Lorentz force mechanism, the SH waves could be generated using a periodic permanent magnet (PPM), producing a bias magnetic field for an aluminum plate [14]–[16]. As the SH0 modal guided wave's excitation source, though the EMAT has a noncontact advantage compared with piezoelectric transducers, its disadvantages on low energy conversion efficiency and low signalto- noise ratio (SNR) could not be ignored. Accordingly, there are many methods to develop the EMAT proposed, including the use of narrowband and ultralow noise receivers, enhanced excitation source, and digital signal optimization processing methods [17], [18]. As a method to modify the transducer structure to improve the energy conversion efficiency, ultrasound wave focusing is widely used in SV body wave focusing, Rayleigh surface wave focusing, and SH guided wave focusing. Ogi et al. [19], [20] developed the line-focusing method of SV waves using continuously varied spacing line sources and applied it to the slit defect detection at the focal line position in the specimen's bottom surface. However, this method could not enable 3-D focusing, and the detection accuracy has not been considered. Besides, point-focusing SV (PFSV) EMAT was proposed by Takishita et al. [21], and they used curved meander line (CML) coils to focus the SV waves on a certain point within the space. Although the transducer's focusing effect is improved, its focusing performance was not studied for the focal area. Furthermore, Thring's new Rayleigh wave EMAT used geometric focusing to detect the surface defect and improve the signal intensity [22]. However, this method is only sensitive to surface defects and is invalid for internal defects.

For SH guided wave focusing method, point-focusing SH (PFSH) EMATs that could focus the waves to a certain point were proposed in our previous studies [23]–[25]. The results showed that the signal intensity was successfully enhanced, and

This work was supported by the National Natural Science Foundation of China (NSFC) under Grant 52077110 and in part by NSFC under Grant 52007088.

Hongyu Sun, Lisha Peng, Shen Wang, Wei Zhao, and Songling Huang are with the State Key Laboratory of Power System, Department of Electrical Engineering, Tsinghua University, Beijing 100084, China (e-mail: huangsling@mail.tsinghua.edu.cn).

Q. Wang is with the Department of Engineering, Durham University, Durham DH1 3LE, U.K.

the performance of a PFSH-EMAT was improved. Specifically, in general, these methods focus on improving the signal intensity by focusing the ultrasound energy in a specific area and exploring past research on improving the signal intensity. However, the focusing accuracy of the EMAT should also be considered. The focal point area's size is a significant factor affecting the detection accuracy and has rarely been reported so far. A larger focal area reduces the intensity of ultrasonic waves and diverges the focal energy, which also reduces the detection accuracy and the imaging resolution. Therefore, the relationship between the focusing performance of the PFSH-EMAT and its different influence parameters should be studied to optimize the focusing capability of the transducer. The orthogonal test as a high-efficiency, fast, and economical test design method has been widely used in many research fields to optimize many influence factors. Besides, the finite-element method (FEM) can obtain conclusions analogous to the experimental results by solving the approximate solutions of the boundary value problems of partial differential equations, thereby reducing the research's complexity. The FEM and orthogonal experiment method can be used together to study the focusing ability of PFSH-EMAT under the influence of multiple parameters.

In this work, the focusing performance of the PFSH-EMAT is investigated by studying different influence parameters on the signal intensity and dimensions of the focal area, and the preliminary research has been published in our conference abstract [26]. The orthogonal test method is used to simplify the analysis process, and the FEM is used to calculate the test results. The signal intensity M, the effective focal length l_{fd}, and the width w_{fd} (focal area dimensions) are considered test results in the test. Seven factors are selected with three levels. Through the range analysis, the factors that offer the greatest impact on M, l_{fd}, and w_{fd} are coil width w, magnet number m, and aperture angle θ, respectively. Considering the signal intensity and the focus area's size, the optimized parameter combination of PFSH-EMAT could be obtained. Moreover, both simulations and experiments show that the parameter-optimized PFSH-EMAT has a better focusing performance than the nonoptimized one.

II. FOCUSING METHOD AND CONFIGURATION

Two mechanisms mainly generate the ultrasonic guided waves in metal plates: the Lorentz force and the other is the magnetostriction. Both the methods generate ultrasonic waves by vibrating the particle of the metal plate in specific directions. However, since the magnetostriction theory does not apply to nonferromagnetic materials, the Lorentz force's excitation is mainly used in the aluminium plate to enable guided waves. For the excitation of the SH waves, a bias magnetic field generated by PPMs is mainly used as an effective method. Fig. 1 shows the configuration of a PPM EMAT. The PPM with four magnets is placed above the aluminium plate and coiled around these magnets. Excitation current with a burst signal is applied on the

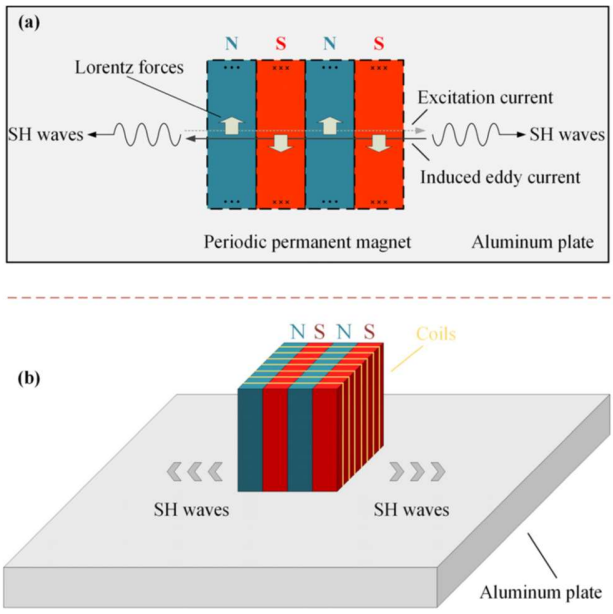

Fig.1. Excitation of SH guided waves with PPM. (a) Top view. (b) 3-D view.

Wire, so the eddy current is induced on the plate surface. Under the effect of the bias periodic magnetic field, pulsed eddy currents will induce Lorentz forces. When forces act on free electrons, the ultrasonic waves will be generated. The symmetrical unfocused SH guided wave transducer in Fig. 1 will simultaneously generate two guided waves that propagate symmetrically to both the sides.

Accordingly, to improve the transducer's performance, the SH ultrasonic guided wave focusing transducer shown in Fig. 2 was designed and proved effective in our previous studies [23]–[25]. Fan-shaped PPM (red and blue sectors) with coils (in yellow) is used to focus SH guided waves at the preset focal point, and all the coils point to the center of the fan-shaped PPM, which is the focal position. A burst current with a bandwidth α and frequency fc is applied to the coils to generate SH guided waves with a certain mode. A single magnet's length is set to half-wavelength (λ/2) to exploit constructive interference phenomena. In this way, the SH guided waves generated by the PFSH EMAT could enable beam focusing and phase focusing simultaneously.

III. ORTHOGONAL TEST AND PARAMETER OPTIMISATION

A. Selection of Parameters and Results

Orthogonal test design is one of the important tools used in parameter analysis [27]. Therefore, it is necessary to determine the factors that need to be tested reasonably. For the SH wave transducer response, the velocity field V(x, z) radiated from a transducer is given as

$$V(x,z)=\int_{-mD/4}^{mD/4}\frac{nI_e}{W}B(x')V_g(x-x')dx' \qquad (1)$$

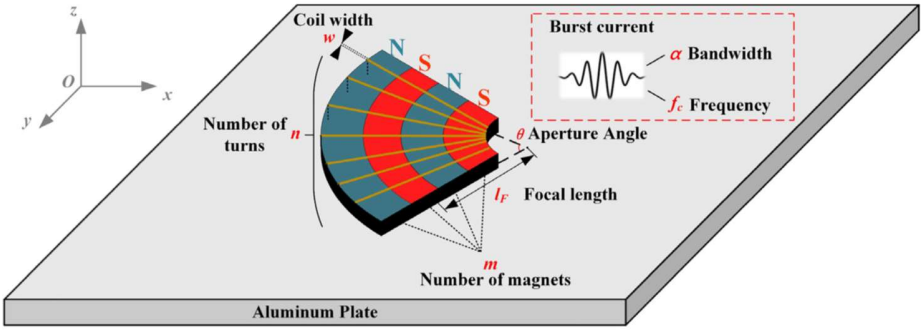

Fig.4. Configuration of a PFSH EMAT.

where m is the magnet number, W is the transducer width, D is the transducer period, n is the coil turns with an excitation current *Ie, B* is the bias magnetic flux density, and *Vg* is the appropriate Green's function. Besides, nI_e/W is the eddy current induced in the specimen.

Since the magnitude, bandwidth, and frequency of the excitation current will affect the mode and amplitude of the SH guided wave, it is also essential to determine the reasonable excitation current properties in the design and optimization of an EMAT. In this work, a burst current is selected as the excitation waveform of the coil, and the expression could be shown as [28]

$$i(t) = I_c e^{-\alpha(t-\tau)^2} \cos[2\pi f_c(t-\tau)+\theta]. \quad (2)$$

Specifically, in this work, the influence parameters are selected: coil turns n, magnet number m, coil width w, excitation current bandwidth α, and frequency *fc*. Aperture angle θ and focal length l_F are also considered in the study as effective impact factors, which are shown in Fig. 2. Current amplitude and lift-off distance will directly affect the amplitude of the wave signal and have been confirmed extensively [19], [20], so they are fixed as constants in this article (current amplitude of 50 A and lift-off distance of 0.5 mm). The three levels for the magnet number m are 4, 6, and 8. The three levels for the coil width *w* are 0.2, 0.4, and 0.6 mm. The three levels for the coil turns *n* are 5, 9, and 13. The three levels for the aperture angle θ are 20◦, 40◦, and 60◦. The three levels for the focal length l_F are 50, 100, and 150 mm. The three levels for the frequency f_c are 500, 600, and 700 kHz. The three levels for the bandwidth factor α are 1, 5, and 9×10^{11} s^{-2}.

For the test results, signal amplitude M is the most critical factor in describing the focusing capability of a PFSH-EMAT, so it is selected as one of the test results. Another important factor in determining the performance of a transducer is its detection accuracy. In a PFSH-EAMT, the dimension of the effective focal area greatly affects the detection accuracy. This is because an excessively large focal area increases detection errors and reduces energy concentration. Therefore, the dimensions of the focal area should be considered in the test design as essential results.

B. Simulation Results and Range Analysis

Introducing the governing equations as completely as possible is required for numerical simulation in the FEM calculation. To describe the physical process of the PFSH-EMAT, Maxwell's equations and elastic dynamic equations are used in the simulation as follows:

$$\sigma\frac{\partial \boldsymbol{A}}{\partial t} - \frac{1}{\mu}\nabla^2 \boldsymbol{A} = \boldsymbol{J}_s. \quad (3)$$

The eddy current *Je* is

$$\boldsymbol{J}_e = -\sigma\frac{\partial \boldsymbol{A}}{\partial t}. \quad (4)$$

As mentioned above, the eddy current *Je* will generate Lorentz force *Fv* in the aluminum plate with a magnetic field *Bs*, and the dynamic magnetic field *Bd* will also affect the Lorentz force

$$\boldsymbol{F}_v = \boldsymbol{J}_e \times (\boldsymbol{B}_d + \boldsymbol{B}_s). \quad (5)$$

Lorentz force *Fv* connects the two physical fields because the external force causes the aluminum plate to be elastically deformed, thereby generating ultrasonic waves by vibration. This process could be described as

$$(\kappa + G)\nabla\nabla\cdot\boldsymbol{u} + G\nabla^2\boldsymbol{u} + \boldsymbol{F}_v = \rho\frac{\partial^2 \boldsymbol{u}}{\partial t^2} \quad (6)$$

where κ and *G* are the Lame constants of the material, ***u*** is the displacement vector, ρ is the material density, and *t* is the time. COMSOL is widely used in scientific research as multiphysical simulation software. The governing equations describing the physical process of the EMATs could be fully described in this software. The joint calculation solves the calculation of Lorentz force using the ac/dc module and the magnetic field (no current) module in this article. Moreover, the solid mechanic module with the linear elastic material is also used. With the coupling of Lorentz force among the various modules, each physical field's calculation will be performed simultaneously and coupled to each other.

As a special case when m = 8, w = 0.6 mm, n = 5, θ = 60◦, l_F = 100 mm, f_c = 500 kHz, and $\alpha = 5 \times 10^{11} s^{-2}$, a simulation is carried out in this article. Fig. 3(a) shows the displacement distribution when SH guided waves reach the focal point, and Fig. 3(b) shows the enlarged figure of the red dotted frame in Fig. 3(a). Fig. 3(c) shows the y-displacement at the focal point, and longitudinal waves appear before shear waves due to their higher velocity. It is shown that the waves are successfully focused at a certain point. Since the focal area's dimensions offer a great influence on defects' detection accuracy,

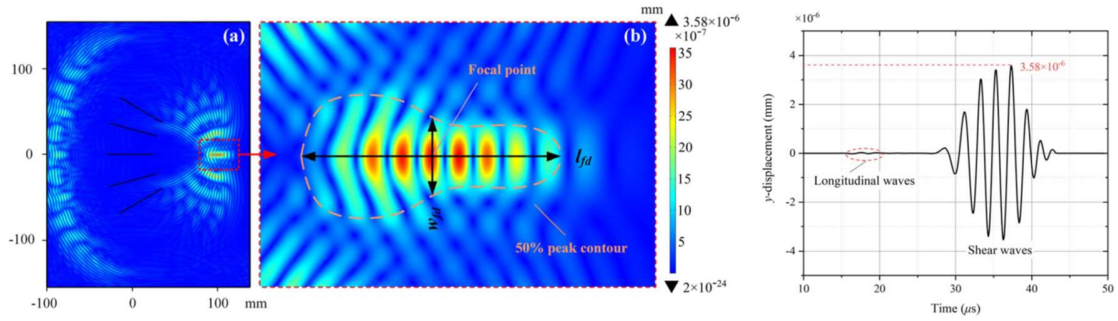

(a,b) (c)

Fig.5. Simulation results for a PFSH-EMAT. (a) Displacement distribution when the waves reach the focal point. (b) Enlarged figure of the red dotted frame. (c) y-displacement at the focal point...

TABLE I

ORTHOGONAL TEST RESULTS FOR COMBINATIONS OF PARAMETERS

Test No.	Factors							Results		
	A	B	C	D	E	F	G	M		
	m	*w*	*n*	*θ*	l_f	f_c	*α*	x10^{-7}	l_{fd}	w_{fd}
	1	mm	1	°	mm	kHz	x10^{11}s^{-2}	mm	mm	mm
1	4	0.20	5	20	50	500	1	26.13	17.19	17.79
2	4	0.40	9	40	100	600	5	37.91	11.60	8.56
3	4	0.60	13	60	150	700	9	44.82	9.91	5.40
4	6	0.20	5	40	100	700	9	7.97	12.09	6.56
5	6	0.40	9	60	150	500	1	66.14	17.94	6.80
6	6	0.60	13	20	50	600	5	129.25	14.73	16.54
7	8	0.20	9	20	150	600	9	13.14	19.88	16.72
8	8	0.40	13	40	50	700	1	137.37	17.17	7.39
9	8	0.60	5	60	100	500	5	35.82	24.96	6.17
10	4	0.20	13	60	100	600	1	35.15	14.93	5.92
11	4	0.40	5	20	150	700	5	14.46	10.14	13.33
12	4	0.60	9	40	50	500	9	73.28	11.90	10.55
13	6	0.20	9	60	50	700	5	25.41	10.94	4.90
14	6	0.40	13	20	100	500	9	53.67	18.26	20.03
15	6	0.60	5	40	150	600	1	45.65	17.46	7.47
16	8	0.20	13	40	150	500	5	26.72	24.45	9.90
17	8	0.40	5	60	50	600	9	23.73	18.46	5.09
18	8	0.60	9	20	100	700	1	101.11	19.01	14.05

TABLE II

RANGE ANALYSIS FOR TEST RESULTS

Results	Level	Factors						
		A	B	C	D	E	F	G
		m	*w*	*n*	*θ*	l_F	f_c	*α*
M (10^{-7} mm)	1	38.59	22.34	25.60	56.10	69.00	46.80	68.48
	2	54.43	55.33	52.70	54.73	45.14	47.41	44.80
	3	56.27	71.57	70.94	38.41	35.10	55.03	35.96
	T_{x1}	17.68	49.23	45.34	17.69	33.90	8.23	32.52
Ljd (mm)	1	12.61	16.58	16.72	16.54	15.07	19.12	17.28
	2	15.24	15.60	15.21	15.78	16.81	16.18	16.14
	3	20.66	16.33	16.58	16.19	16.63	13.21	15.09
	T_{x2}	8.05	0.98	1.51	0.76	1.74	5.91	2.20
W_{fd} (mm)	1	10.26	10.30	9.40	16.41	10.31	11.87	9.90
	2	10.38	10.20	10.26	8.41	10.22	10.05	9.90
	3	9.89	10.03	10.86	5.71	9.94	8.61	10.73
	T_{x3}	0.49	0.27	1.46	10.70	0.44	3.26	0.83

a reasonable quantitative standard method needs to be proposed. Therefore, the area enclosed by the 50% peak contour is defined as the effective focal area shown in Fig. 3(b). The parameters that could describe the focal area dimensions are also shown. The x-axis direction's length is the effective focal length lfd, and the width in the y-axis direction is the effective focal width wfd. Accordingly, the effective focal length l_{fd}, and the effective focal width w_{fd} are selected as the additional two test results of the orthogonal test.

For an orthogonal test with seven factors and three results, an L18 (37) orthogonal table is selected in the test. Using the above methods, the test results at different levels of different factors could be obtained through numerical simulations, as shown in Table I. The results of the range analysis are shown in Table II. Fig. 4 shows the average values from the test results and influence degrees from the range analysis results of the seven factors with three levels.

For signal amplitude *M*, Fig. 4 shows that the three factors that offer the most significant impact are the coil width *w*, coil turns n, and focal length l_F (approximately equivalent to bandwidth factor α). It could be observed that *M* increases with w and n and decreases with lF and α. Therefore, to improve the focusing intensity of the PFSH-EMAT, *w* and *n* should be set larger, while l_F and *α* should be lower.

For effective focal length l_{fd}, the three factors that exhibit the greatest impact are magnet number *m*, frequency *fc*, and bandwidth factor α. It shows that l_{fd} increases with m and decreases with *fc* and *α*. Therefore, to reduce the focal area dimension, m should be smaller, while *fc* and *α* should be larger

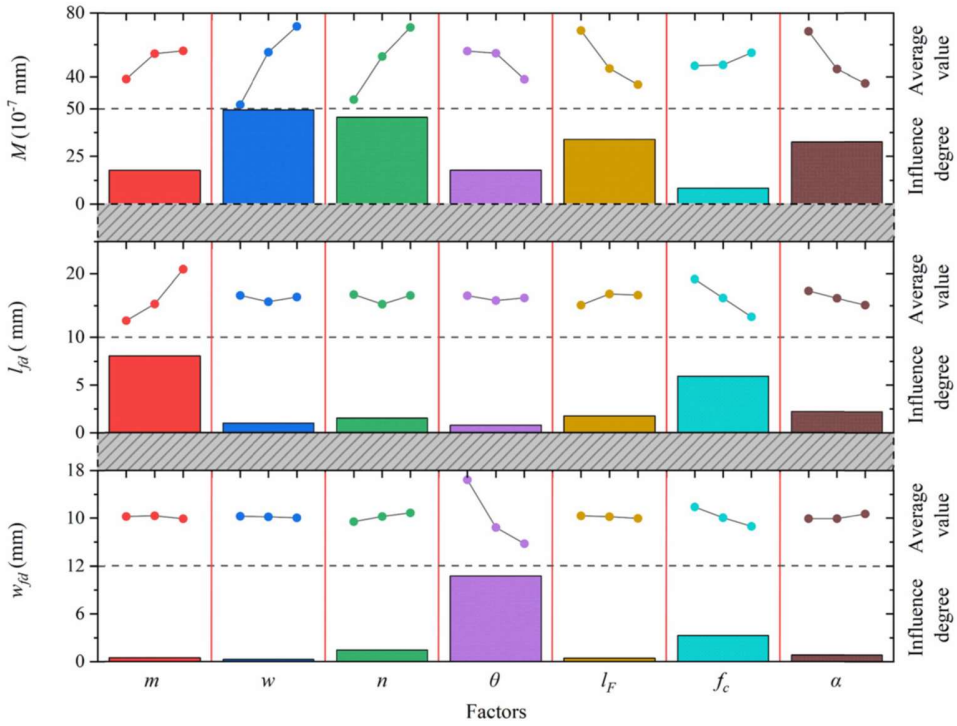

Fig.4. Orthogonal test results and range analysis for different factors with different levels.

TABLE III
SIMULATION RESULTS FOR OPTIMIZED TEST AND AVERAGE RESULTS FOR TEST No. 1-18

Results	M (X10^{-7}MM)	l_{fd} (mm)	W_{fd} (mm)
Optimized test	121.60	10.05	5.03
Average of 1-18	49.75	16.17	10.18

For effective focal width w_{fd}, the three factors that have the greatest impact are the aperture angle θ, frequency *fc*, and coil turns *n*. It is shown that w_{fd} increases with n and decreases with *fc* and θ. Specifically, to reduce the focal area dimension, θ and *fc* should be larger, while *n* should be smaller.

C. Selection of Parameters and Results

To achieve better performance of the PFSH-EMAT, the parameters studied above should be reasonably combined. To enable high focusing intensity and high detection accuracy, the influence of various factors should be considered comprehensively. It is clearly shown in Fig. 4 that factors w, n, l_F, and α have a greater influence on *M*, but less on l_{fd} and w_{fd}. Similarly, factors m and fc dominate l_{fd}, and θ has the highest influence degree on w_{fd}. Accordingly, the optimized parameter combination should be selected as follows: $m = 4$, $w = 0.6$ mm, $n = 13$, $\theta = 60°$, $l_F = 50$ mm, $fc = 700$ kHz, and $\alpha = 1\times10^{11}$ s^{-2}. The simulation results for this optimized test are shown in Table III, and the average results for the test No. 1–18 are also calculated and shown. It can be seen that the signal amplitude of the optimized test at the focal point is nearly 144% higher than the average of all the tests, lfd decreased by 38%, and w_{fd} decreased by 51%. Therefore, the parameter-optimized PFSH-MAT has a better focusing performance. It could be predicted

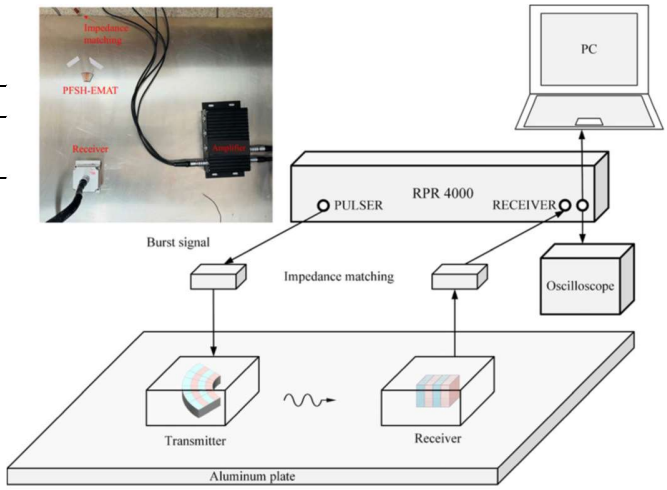

Fig.5. Experiment configuration of a PFSH-EMAT..

It could be predicted that more levels could make the selection of parameters more accurate, and the optimization effect will be better.

IV. EXPERIMENTS

To verify the optimization results' effectiveness, the parameters' combination of test No. 7 is selected as a comparison. Fig. 5 shows the experiment configuration, PFSH-EMAT, and the receiving EMAT is placed above the aluminum plate. RPR- 4000 is widely used as an ultrasonic excitation source and receiving device in ultrasonic guided wave detection. It could transmit the pulses of a specified waveform (burst signal) and pass it through the matching impedance to the transmitter.

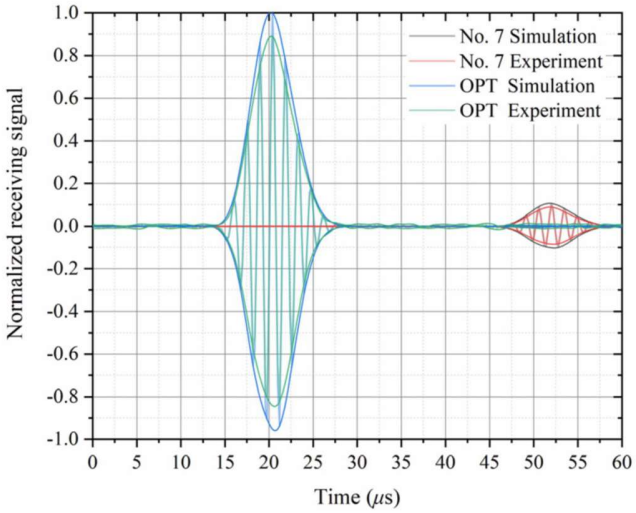

Fig.6. Normalized receiving signal for optimized test and nonoptimized test No. 7.

TABLE IV
EXPERIMENTAL RESULTS FOR ALL TESTS AND THE ERRORS COMPARED WITH THE SIMULATION RESULTS

Test No.	Normalized M	M error (%)	L_{fd}	L_{fd} error (%)	W_{fd}	W_{fd} error (%)	Mean error (%)
1	0.17	10.77	16.46	4.28	18.32	2.95	6.00
2	0.32	15.67	12.32	6.16	8.99	5.02	8.95
3	0.19	41.90	10.62	7.11	4.87	9.91	19.64
4	0.08	37.52	12.00	0.74	6.79	3.51	13.92
5	0.42	12.82	18.29	1.92	6.87	1.03	5.26
6	0.89	5.48	14.30	2.95	16.39	0.91	3.11
7	0.11	15.04	21.80	2.49	15.40	4.75	7.43
8	1.00	0.00	16.67	2.91	8.38	13.40	5.44
9	0.33	26.28	25.51	2.18	6.76	9.48	12.65
10	0.23	10.36	15.32	2.61	5.37	9.38	7.45
11	0.14	33.19	9.52	6.11	12.39	7.09	15.47
12	0.39	27.01	11.51	3.32	10.14	3.93	11.42
13	0.18	1.36	11.35	3.75	5.49	12.04	5.72
14	0.27	30.21	18.62	1.94	20.00	0.15	10.77
15	0.31	6.86	17.54	0.43	7.35	1.67	2.99
16	0.17	12.77	23.54	3.72	9.03	8.79	8.43
17	0.21	21.39	19.21	4.04	6.07	19.16	14.86
18	0.69	6.41	18.52	2.60	13.82	1.64	3.55

The SH waves are then excited by the PFSH-EMAT and focused at the focal point where the receiver locates, and the experimental and simulated parameters are kept the same. Next, the received signal is transmitted to RPR-4000 again through the same impedance matching, and the received signal could therefore be displayed on the oscilloscope and processed on the PC. In the experiment, the PPM is Nd-Fe-B magnets and processed into a special shape to generate a focused ultrasonic guided wave. In the coil winding process, we tried our best to make the bottom coil fit the sector-shaped permanent magnet as flatly as possible to increase the intensity of the excited ultrasonic signal. The aluminum plate has a size of 500 × 500 × 1 mm^3 and a burst current is applied to the coils with a 50-A amplitude through the power programming method, and the waveform of the output current could also be monitored. Fig. 6 shows the simulated and experimental results of two PFSH-EMATs with different parameter combinations. Normalized signals at focal points are shown and waveform envelopes are added to make the results clearer. Due to the different focal lengths, the moments at which the ultrasonic guided waves reach the focal points are different: The transducer with optimized parameters generates waveforms around 20 μs, and those around 52 μs are the results for test No. 7. The two simulations show good agreement with experiments, though the experiment results are slightly lower, resulting in unavoidable errors. Accordingly, the wave amplitude at the focal point of a PFSH-EMAT could be measured.

To obtain the dimensions of the focal area, effective focal length l_{fd} and width w_{fd} are required. In the experiment, the value of the effective focal length l_{fd} could be obtained by changing the horizontal position of the receiving transducer until the received ultrasonic signal is equal to half the signal intensity at the focal point. Besides, the effective focal width w_{fd} could also be obtained. The results show that the signal intensity of the optimized PFSH-EMAT is nearly ten times the nonoptimized one. For the focal area dimensions, the experiment results of the optimized PFSH-EMAT are l_{fd} = 14.5 mm and w_{fd} = 4.2 mm. Moreover, the experiment results of the nonoptimized one (test 7) are l_{fd} = 21.8 mm and w_{fd} = 15.4 mm. Specifically, the transducer with optimized parameters could effectively reduce the focal area. Table IV shows the normalized signal intensity and focal area dimensions under all test parameter combinations. It can be seen from Table IV that the error between the experimental result and the simulation result is relatively small, and the amplitude error between some groups is large (about 20% or more); this is due to the low SNR caused by low signal intensity.

V. CONCLUSIONS

In this work, the orthogonal test method is used to study the focusing performance of a PFSH-EMAT. The test results are obtained by 3-D FEM simulation with different factors of different levels. Signal intensity M and focal area dimensions l_{fd} and w_{fd} are selected as the concerning results. An L18(37) orthogonal table with seven factors of three levels is used, and range analysis is performed to obtain each factor's influence degree.

The results show that for signal amplitude M, the top three impact factors are the coil width w, coil turns n, and focal length l_F (equal to bandwidth factor α). For effective focal length l_{fd}, the top three impact factors are the magnet number m, frequency fc, and bandwidth factor α. For effective focal width w_{fd}, the top three impact factors are the aperture angle θ, frequency fc, and coil turns n. To improve the focusing intensity of the PFSH-EMAT, w and n should be set larger, while l_F and α should be set lower. To enable high detection accuracy, m should be set smaller, while θ and fc should be set larger, so the focal area dimensions will be smaller. Therefore, considering the influence of different parameter combinations on the focused signal intensity and the detection accuracy, the optimized parameter combination of PFSH-EMAT is obtained. The optimized test's signal intensity at the focal point is nearly 144.42% higher than the average of all the tests, l_{fd} decreased by 38.84%, and w_{fd} decreased by 50.59%. The experiment also verified that the transducer with optimized parameters has a significant focusing performance. Therefore, the focal area dimension optimization method proposed in this article can guide the design of focusing transducers, thereby improving the

energy conversion efficiency of EMAT and making it more potential in small defect detection.

REFERENCES

[1] M. Hirao and H. Ogi, "An SH-wave EMAT technique for gas pipeline inspection," *NDT & E Int.,* vol.32, no.3, pp.127-132, Apr. 1999.

[2] S. Wang, S. Huang, Y. Zhang, and W. Zhao, "Multiphusics modelling of a Lorentz force-based meander coil electromagnetic acoustic transducer via steady-state and transient analysis," *IEEE Sensors J*., vol. 16, no.17, pp.6641-6651, Sep.2016.

[3] S. Legendre, D. Massicotte, J. Goyette, and T. K. Bose, "Neural classification of lamb wave ultrasonic weld testing signals using wavelet coefficients," IEEE Trans. Instrum. Meas., vol. 50, no.3, pp.672-678, Jun, 2001.

[4] P. H. Carr, "The generation and propagation of acoustic surface waves at microwave frequencies," IEEE Trans. Microw. Theory Techn., vol.MTT-17, no. 11, pp.845-855, Nov. 1969.

[5] H. Ogi, M. Hirao, T. Honda, and H. Fukuoka, "Ultrasonic diffraction from a transducer with arbitrary geometry and strength distribution," J. Acoust. Soc. Amer., vol98, no.2, pp.1191-1198, Aug. 1995.

[6] P. A. Petcher and S. Dixon, "Weld defect detection using PPM EMAT generated shear horizontal ultrasound," *NDT E Int.*, vol.74, pp.58-65, Sep.2015.

[7] J. J. da Silva, M. G. Wanzeller, P. de Almeida Farias, and J. S. da Rocha Neto, "Development of circuits for excitation and reception in ultrasonic transducers for generation of guided waves in hollow cylinders for fouling detection," IEEE Trans. Instrum. Meas., vol.57, no.6, pp. 1149-1153, Jun.2008.

[8] R. B. Thompson, "Generation of horizontally polarized shear waves in ferromagnetic materials using magnetostrictively coupled meander-coil electromagnetic transducers,"Appl.Phys. Lett., vol.34, no.2, pp. 175-177, Jan. 1979.

[9] H. Kwun and C. M. Teller, "Magnetostrictive generation and detection of longitudinal torsional, and flexural waves in a steel rod," J. Acoust. Soc Amer., vol. 96, no.2, pp.1202-1204, Aug. 1994.

[10] H. Kwun and K. A. Bartels, "Magnetostrictive sensor technology and its applications," Ultrasonics, vol. 36, no. 1-5, pp.171-178, Feb. 1998.

[11] R. Murayama, S. Makiyama, M. Kodama, and Y. Taniguchi," Development of an ultrasonic inspection robot using an electromagnetic acoustic transducer for a Lamb wave an an SH-plate wave," *Ultrasonics*, vol.42, nos.1-9, pp.825-829, Apr.2004.

[12] P. A. Petcher, S. E. Burrows, and S. Dixon, "Shear horizontal (SH) ultrasound wave propagation around smooth corners," Ultrasonics, vol. 54, no.4, pp.997-104, 2014.

[13] Z. Wei, S. Huang, S. Wang, and W.Zhao, "Magnetostriction-based omni-directional guided wave transducer for high-accuracy tomography of steel plate defects," IEEE Sensors J., vol. 15, no.11, pp.6549-6558, Nov. 2015.

[14] C. F. Vasile and R. B. Thompson, "Excitation of horizontally polarized shear elastic waves by electromagnetic transducers with periodic permanent magnets," *J. Appl. Phys.,* vol.50, no.4, pp.2583-2588, Apr. 1979.

[15] B. W. Maxfield and C. M. Fortunko, "The design and use of electro-magnetic acoustic wave transducers (EMATs)" Mater. *Eval.,* vol. 41, pp.1399-1408, Nov. 1983.

[16] R. Ribichini, F. Cegla, P. Nagy, and P. Cawley, "Study and comparison of different EMAT configuration for SH wave inspection," *IEEE Trans. Ultrason., Ferroelectr., Freq. Control*, vol. 58, no.12, pp. 2571-2581, Dec.2011.

[17] S. E. Burrows, Y. Fan, and S. Dixon, "High temperature thickness measurements of stainless steel and low carbon steel using electromagnetic acoustic transducers," NDT E Int., vol.68, pp.73-77, De.2014.

[18] N. Lunn, S.Dixon, and M. D. G. Potter, "High temperature EMAT design for scanning or fixed point operation on magnetite coated steel," *NDT & E Int*., vol.89, pp.74-80, Jul. 2017.

[19] H. Ogi, M. Hirao, and T. Ohtani, "Line-focusing of ultrasonic SV wave by electromagnetic acoustic transducer," *J. Acoust. Soc. Amer.,* vol. 103, no.5, pp2411-2415, May 1998.

[20] H. Ogi, M. Hirao, and T. Ohtani, "Line-focusing electromagnetic acoustic transducers for the detection of slit defects," IEEE Trans. Ultrason Ferr., vol. 46, no.2, pp.341-346, Mar.1999.

[21] T. Takishita, K. Ashida, N. Nakamura, H. Ogi, and M. Hirao, "Development of shear-vertical-wave point-focusing electromagnetic acoustic transducer*," Jpn. J. Appl. Phys.,* vol. 54, no. 7S1, P. 07HC04, 2015.

[22] C. B. Thring, Y. Fan, and R. S. Edwards, "Multi-coil focused EMAT for characterization of surface-breaking defects of arbitrary orientation," *NDT & E Int.*, vol.88, pp. 1-7, Jun. 2017.

[23] H. Sun, S. Wang, S. Huang, Q. Wang, and W.Zhao, "Point-focusing of shear-horizontal wave using fan-shaped periodic permanent magnet focusing coils EMAT for plate inspection., *IEEE Sensors J*., vol. 19, no.12, pp.4393-4404, Jun. 2019.

[24] H. Sun, S. Huang, Q.Wang, S. Wang, and W. Zhao, "Improvement of unidirectional focusing periodic permanent magnet shear-horizontal wave electromagnetic acoustic transducer by oblique bias magnetic field," *Sens. Actuators A, Phys.,* vol 290, pp.36-47, May 2019.

[25] S. L.Huang, H. Y. Sun, Q. Wang, S. Wang, and W. Zhao, "Unidirectional focusing of horizontally polarized shear elastic waves electromagnetic acoustic transducers for plate inspection," *J. Appl. Phys.,* vol. 125, no.16, Appr.2019, Art, no. 164504.

[26] H. Sun, L. Peng, S. Wang, Q. Wang, W. Zhao, and S. Huang, "Effective focal area dimension optimization of shear-horizontal point-focusing EMAT using orthogonal test method," in Proc. Conf. Precis. Electromagn, Meas. (CPEM), Aug. 2020, pp.1-2.

[27] X. Jia and Q. Ouyang, "Optimal design of point-focusing shear vertical wave electromagnetic ultrasonic transducers based on orthogonal test method," *IEEE Sensors J*.,vol. 18, no.19, pp. 8064-8073, Oct. 2018.

[28] H. Sun, L.Peng, S. Huang, Q. Wang, S. Wang, and W. Zhao, "Analytical model and optimal focal position selection for oblique point-focusing shear horizontal guided wave EMAT," Construct. Builing Mater., vol. 258, Oct.2020, Art. no. 120375.